J. Fluid Mech. (1988), *vol.* 197, *pp.* 523–549
Printed in Great Britain

Equilibrium shapes and stability of captive annular menisci

By J. A. TSAMOPOULOS†, A. J. POSLINSKI AND M. E. RYAN
Department of Chemical Engineering, State University of New York at Buffalo, Buffalo, NY 14260, USA

(Received 23 December 1987)

Equilibrium shapes and stability of annular fluid menisci held together by surface tension are analysed by applying asymptotic and computer-aided techniques from bifurcation theory. The shapes and locations of the menisci are governed by the Young–Laplace equation. These shapes are grouped together into families of like symmetry that branch from the basic family of annular shapes at specific values of the aspect ratio, α. Multiple equilibrium shapes exist over certain values of α. The inner, outer or both the inner and outer interfaces may possess either a cylindrical or sinusoidal equilibrium shape. Changes in applied pressure, fluid volume, or gravitational Bond number break families of the same symmetry which now develop limit points. Numerical calculations rely on a finite-element representation of the interfaces and the results compare very well with asymptotic analysis which is valid for small deformations. The results are important for the blow moulding process and are invaluable in understanding its dynamics. These dynamics are expected to be considerably different from the dynamics of a liquid jet first analysed by Rayleigh.

1. Introduction

Deformation of fluid menisci plays an important role in many commercial processes such as coating and film flows employed in various heat and mass transfer operations. Coating of solids is commonly encountered in the manufacture of photographic films. In addition, blow moulding and thermoforming constitute two important polymer processing operations in which a softened polymeric membrane is formed into a thin-walled plastic container or structural part. The blow moulding process involves the inflation of a hollow cylindrical tube within a mould cavity that possesses the desired shape of the finished product. In a typical thermoforming process a heated plastic sheet is clamped over a mould and forced by external pressure to deform and contact the mould surface. In both operations the shape and stability of the fluid meniscus plays an important role in determining the time evolution of the free surface of the fluid and the quality of the finished product. The final wall thickness distribution of either a blow moulded or thermoformed part, the optimal use of material, the evaluation of design concepts, and the comparison of process alternatives necessitates the development of a realistic dynamic simulation of the inflation or deformation process. Prior to this undertaking however, the dependence of static equilibrium shapes and stability of the annular menisci on multiple parameters must be fully understood. Furthermore, the interest in annular menisci has been recently motivated by the production of lithium shields to be used in certain pulsed fusion reactors. In particular, Esser, Paul & Abdel-Khalik (1981)

† Author to whom correspondence should be addressed.

derived the dispersion relation to predict the range of disturbance frequencies leading to instability. In addition, Lee & Wang (1986) have analysed, and Hoffman, Takahashi & Monson (1980) have performed experiments to determine, the length required for closure of a vertical annular water jet due to the action of surface tension forces.

The equilibrium shape of an interface separating two immiscible fluids is governed by the much-studied equation of Young (1805) and Laplace (1805) which equates the capillary force acting on the interface to the pressure force exerted by the bulk fluid on either side. At equilibrium these forces are conservative and the equilibrium shape can be derived by making the total potential energy stationary with respect to small changes in the shape. Under this condition the shape is stable if the stationary point is a local minimum with respect to all small perturbations, and unstable if the stationary point is a local maximum. Alternatively, interfacial stability can be determined by solution of an eigenvalue problem arising from small-amplitude analysis of the Young–Laplace equation.

Ideas and methodology from the field of bifurcation theory have been applied with success to interfacial problems controlled by single or multiple parameters; see Ungar & Brown (1982) and references therein. The asymptotic methods used here are based on the perturbation procedures described in Ioos & Joseph (1980) and Matkowsky & Reiss (1977), and they are designed to account for the splitting and shifting of bifurcation points as secondary parameters are varied. The numerical methods combine finite-element representation (Strang & Fix 1973) of the meniscus shape with computer-implemented techniques for tracking shape families as explained in Keller (1977) and Abbott (1978). Within this framework, the stability of the menisci to steady bifurcating solutions can be directly inferred from the connectivity of the shape families. Thus, any explicit eigenvalue calculations, used elsewhere (Brown & Scriven 1980), can be circumvented.

Of special relevance for the present work is Rayleigh's (1879, 1892) analysis (see also Chandrasekhar 1961) on the stability of a cylindrical jet. As Plateau (1873) first showed, this instability is caused by surface tension forces which make the infinite cylinder at equilibrium unstable with respect to separated droplets which have less surface area than the original cylinder. It is now well known that a liquid cylinder is neutrally stable to a shape disturbance that is infinitesimal in amplitude, sinusoidal in shape, and of wavelength equal to the circumference of the cylinder. Furthermore, the cylindrical fluid column is unstable to disturbances of even greater wavelength and the evolution in time of unstable shapes depends on the mode of maximum instability.

The existence of neutrally stable shapes indicates that two or more shape families intersect each other at the so-called critical or bifurcation points. In general, the new shape family may be stable or unstable depending on the potential energy at equilibrium, and bifurcation theory provides a useful tool to systematize the analysis. Mathematically stable shapes constitute possible configurations, whereas unstable shapes are not physically realizable, but influence the stability of nearby equilibrium shapes, especially when multiple parameters are involved. In the cylindrical jet, all critical points correspond to subcritical bifurcations between the families of cylindrical interfaces and deformed static shapes. Thus, according to bifurcation theory, the cylindrical shape is unstable with respect to disturbances with wavelength larger than the first critical one. Similarly, all static shapes that belong to the bifurcating families are unstable. In addition, weakly nonlinear dynamic analysis has shown that the critical wavelength depends on the square of

the amplitude of the disturbance (Nayfeh 1970). In contrast to the above, if the first critical point corresponds to a transcritical bifurcation, the unperturbed shapes would still become unstable there, but shapes in the bifurcating family with larger wavelengths would be stable. Moreover, the critical wavelength would vary linearly with the amplitude of the disturbance. Indeed, this situation arises in the study of break-up of a charged drop, where neutral equilibrium is achieved when cohesive surface tension forces are counterbalanced by electrostatic repulsion (Tsamopoulos, Akylas & Brown 1985).

One of the goals of the present analysis is to determine which of the two markedly different bifurcation structures is exhibited by annuluar menisci. Specifically, it will be shown that the captive annular mesniscus becomes unstable owing to capillary forces when the ratio of its height to its outer radius exceeds a certain critical value. The inner, outer or both interfaces of menisci that belong to bifurcating families may be sinusoidal. Also, the first critical point corresponds to a transcritical bifurcation, which is contrary to what is intuitively expected by analogy with the cylindrical jet. In addition, when the pressure applied on the inner surface of the annular meniscus is increased, or the volume of the fluid is decreased, the annular-like shape family smoothly connects with the first bifurcating one and remains stable past the first critical point. However, when the pressure is decreased or the fluid volume increased, the annular-like shape family terminates prior to the first critical point. The extent to which stable static families exist depends also on the thickness of the meniscus and must be known before dynamic simulations or new experimental designs are undertaken. This type of analysis has not been undertaken before, although a quantitative study of annular liquid jets was first performed by Boussinesq (1869).

Force balances at equilibrium for the two interfaces of the meniscus are presented in §2. The family of cylindrical shapes along with the perturbed surfaces are derived in §3. These are the asymptotic solutions to the above-mentioned set of coupled equations when only small deformations are allowed. An extension of the bifurcating shape families in the nonlinear regime requires numerical simulation and this is carried out in §4. In the same section, the unfolding of the bifurcations due to variations in pressure, fluid volume, and gravity is considered. Finally, comparison and discussion of the results and their implications for stability are given in §5.

2. Governing equations

Consider a liquid annular meniscus of volume $\tilde{V}$ fixed at both ends by contact with stationary solid surfaces situated at a distance $\tilde{L}$ from each other. The liquid wets the two solid surfaces and forms two fixed, concentric and circular contact lines on each surface, the outer one having radius $\tilde{r}_{\mathrm{O}}$ and the inner one $\tilde{r}_{\mathrm{I}} = \tilde{r}_{\mathrm{O}} - \tilde{\delta}_0$, where $\tilde{\delta}_0$ is the thickness of the contact surface. As shown in figure 1, the centres of the two contact surfaces lie on the same vertical axis. In addition, pressure acts uniformly on the inner and outer liquid/air interfaces and gravity acts downwards. The inner and outer interfaces of the liquid meniscus are given by $\tilde{R}_{\mathrm{I}} = \tilde{R}_{\mathrm{I}}(\tilde{z}, \theta)$ and $\tilde{R}_{\mathrm{O}} = \tilde{R}_{\mathrm{O}}(\tilde{z}, \theta)$, respectively in the Monge cylindrical representation. The force balance for each interface is given by a generalization of the Young–Laplace equation to include the gravitational potential. Thus

$$(P_{\mathrm{I}} - P_{\mathrm{F}}) + Bz + 2\mathscr{H}_{\mathrm{I}} = 0, \tag{2.1}$$

$$(P_{\mathrm{F}} - P_{\mathrm{O}}) - Bz + 2\mathscr{H}_{\mathrm{O}} = 0, \tag{2.2}$$

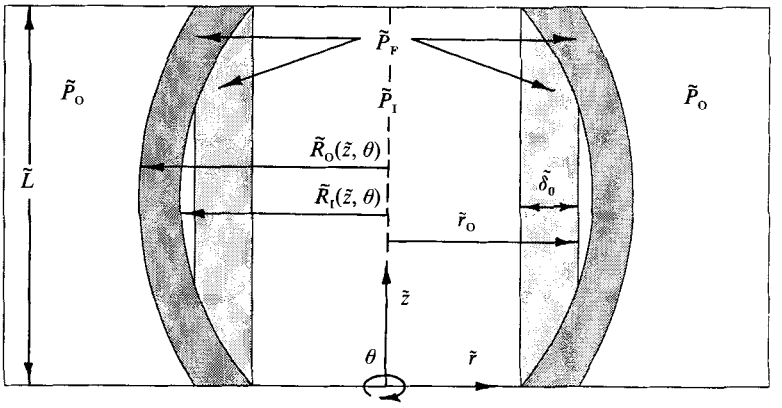

FIGURE 1. Schematic representation of the annular meniscus.

where $P_{I,F,O} \equiv \tilde{r}_O \tilde{P}_{I,F,O}/\sigma$ denote the dimensionless pressures of the inner gas phase, the liquid phase, and the outer gas phase respectively, $B \equiv \tilde{r}_O \tilde{L} \Delta\rho\, g/\sigma$ is the gravitational Bond number, $z = \tilde{z}/\tilde{L}$ is the dimensionless vertical distance and $\mathscr{H}_{I,O} = \tilde{\mathscr{H}}_{I,O} \tilde{r}_O$ denotes the mean curvature of the inner and outer surfaces, respectively. In these definitions σ is the surface tension for either interface, $\Delta\rho \equiv \rho_F - \rho_G$ is the density difference between the liquid and the surrounding medium, and g is the acceleration due to gravity. The expression for the mean curvature $\mathscr{H}$ written in terms of any surface with radial representation $F(z,\theta)$ is given by

$$2\mathscr{H} = -\frac{2\alpha^2 F_\theta F_z F_{z\theta} - \alpha^2 F_{zz}(F^2 + F_\theta^2) + F(1 + \alpha^2 F_z^2 + 2F_\theta^2/F^2) - F_{\theta\theta}(1 + \alpha^2 F_z^2)}{F^2(1 + \alpha^2 F_z^2 + F_\theta^2/F^2)^{\frac{3}{2}}}, \quad (2.3)$$

where $\alpha \equiv \tilde{r}_O/\tilde{L}$ is the aspect ratio of the undeformed annulus and the subscripts z and θ denote partial differentiation with respect to that coordinate. It should be noted that the corresponding expressions given by Brown & Scriven (1980) and Ungar & Brown (1982) have minor typographical errors. This expression reduces to the required forms for the inner and outer interfaces by substituting $R_I(z,\theta) = \tilde{R}_I(\tilde{z},\theta)/\tilde{r}_O$ and $R_O(z,\theta) = \tilde{R}_O(\tilde{z},\theta)/\tilde{r}_O$, respectively for $F(z,\theta)$ in (2.3). When (2.1) and (2.2) are derived as the Euler equations of the appropriate energy minimization problem, the reference pressure difference, or equivalently here P_F, arises as the Lagrange multiplier for constraining the liquid meniscus to have constant dimensionless volume $V = \tilde{V}/(\pi \tilde{r}_O^2 \tilde{L})$. As a result, this final unknown is determined from the following constraint:

$$V = \frac{1}{2\pi} \int_0^{2\pi} \int_0^1 (R_O^2 - R_I^2)\, dz\, d\theta. \quad (2.4)$$

Where the meniscus intersects the solid surfaces three different types of boundary conditions are possible: the contact line is specified; the contact angle is specified; or the location of contact and the angle are related. In the present analysis it is assumed that the liquid wets the solid at the edges of two concentric circles but is not allowed to slip, so that

$$R_O(0,\theta) = R_O(1,\theta) = 1, \qquad 0 \leqslant \theta \leqslant \pi, \quad (2.5)$$

$$R_I(0,\theta) = R_I(1,\theta) = 1 - t, \quad 0 \leqslant \theta \leqslant \pi, \quad (2.6)$$

where $t \equiv \tilde{\delta}_0/\tilde{r}_0$ is the dimensionless thickness of the original meniscus. Finally, all shapes must be periodic in the azimuthal direction with periodicity 2π:

$$R_0(z,0) = R_0(z,2\pi), \qquad 0 \leqslant z \leqslant 1, \tag{2.7}$$

$$R_{0,\theta}(z,0) = R_{0,\theta}(z,2\pi) = 0, \quad 0 \leqslant z \leqslant 1, \tag{2.8}$$

$$R_1(z,0) = R_1(z,2\pi), \qquad 0 \leqslant z \leqslant 1, \tag{2.9}$$

$$R_{1,\theta}(z,0) = R_{1,\theta}(z,2\pi) = 0, \quad 0 \leqslant z \leqslant 1. \tag{2.10}$$

3. Perturbation solutions about the annular meniscus

When no external forces are present the meniscus can assume the shape of a perfect cylindrical annulus for all aspect ratios and thicknesses. Consequently, $B = 0$, $V = t(2-t)$ and the solution to (2.1)–(2.10) is

$$R_0(z,\theta) = 1, \quad R_1(z,\theta) = 1-t, \quad P_F - P_0 = 1, \quad P_I - P_F = \frac{1}{1-t}. \tag{3.1}$$

By setting the outer pressure to zero the inner pressure is given by

$$P_I = \frac{2-t}{1-t} + \Delta P, \tag{3.2}$$

where the first term on the right-hand side of (3.2) is required to balance the surface tension forces in order to maintain the perfect annular shape. The second term in (3.2) is presently zero, but in general represents the externally applied pressure that causes the annulus to deform.

Following Ungar & Brown (1982), the equilibrium shapes and stability of the liquid meniscus subject to variations in the aspect ratio, external pressure, fluid volume and gravity are obtained by a double expansion of the unknowns ($R_0(z,\theta)$, $R_1(z,\theta), P_F$) and the parameters ($\alpha, \Delta P, \Delta V, B$). Thus,

$$\begin{bmatrix} R_0(z,\theta;\epsilon,\gamma) \\ R_1(z,\theta;\epsilon,\gamma) \\ P_F(\epsilon,\gamma) \\ \alpha(\epsilon,\gamma) \\ \Delta P(\epsilon,\gamma) \\ \Delta V(\epsilon,\gamma) \\ B(\epsilon,\gamma) \end{bmatrix} = \sum_{n=0}^{\infty}\sum_{m=0}^{\infty} \epsilon^n \gamma^m \begin{bmatrix} R_0^{(n,m)}(z,\theta) \\ R_1^{(n,m)}(z,\theta) \\ P_F^{(n,m)} \\ \alpha^{(n,m)} \\ \Delta P^{(n,m)} \\ \Delta V^{(n,m)} \\ B^{(n,m)} \end{bmatrix} \tag{3.3}$$

where $\Delta V = V - t(2-t)$. The first coefficient in the expansions, ϵ, measures the difference between each bifurcating shape and the original annular shape, whereas the second variable, γ, is used to scale the departure of a particular bifurcating family from its initial position when additional parameters are varied ($\Delta P, \Delta V, B$). As shown in §4 these parameters scale differently with γ. The identifying exponent, (n,m), gives the order of the expansion in terms of ϵ and γ.

The asymptotic analysis if greatly expedited by the use of the symbolic manipulator MACSYMA (1977). The first term in each expansion is characterized by the exponent $(0,0)$ and corresponds to the base solution of the cylindrical annulus given by (3.1). Initially, axisymmetric disturbances are considered. Substituting

(3.3) into (2.1)–(2.4) yields at each order the following coupled set of linear ordinary differential equations:

$$\frac{\mathrm{d}^2 R_{\mathrm{I}}^{(n,m)}}{\mathrm{d}z^2} + \mu^2 R_{\mathrm{I}}^{(n,m)} - \delta^2 P_{\mathrm{F}}^{(n,m)} = d_{\mathrm{I}}^{(n,m)}, \tag{3.4}$$

$$\frac{\mathrm{d}^2 R_{\mathrm{O}}^{(n,m)}}{\mathrm{d}z^2} + \delta^2 R_{\mathrm{O}}^{(n,m)} + \delta^2 P_{\mathrm{F}}^{(n,m)} = d_{\mathrm{O}}^{(n,m)}, \tag{3.5}$$

$$\int_0^1 [R_{\mathrm{O}}^{(n,m)} - (1-t) R_{\mathrm{I}}^{(n,m)}]\,\mathrm{d}z = d_{\mathrm{P}}^{(n,m)}, \tag{3.6}$$

where $\mu = 1/[\alpha^{(0,0)}(1-t)]$, $\delta = 1/\alpha^{(0,0)}$ and $d_{\mathrm{I,O,P}}^{(n,m)}$ are the non-homogeneous terms in the equations that involve lower-order terms from the expansion (3.3). At first order in ϵ they are zero and at first order in γ they are given as follows:

$$\begin{bmatrix} d_{\mathrm{I}}^{(0,1)} \\ d_{\mathrm{O}}^{(0,1)} \\ d_{\mathrm{P}}^{(0,1)} \end{bmatrix} = \begin{bmatrix} -\delta^2(B^{(0,1)}z + \Delta P^{(0,1)}) \\ \delta^2 B^{(0,1)} z \\ \tfrac{1}{2}\Delta V^{(0,1)} \end{bmatrix}. \tag{3.7}$$

The derivation of the non-homogeneous terms at higher orders is tedious but straightforward. However, these terms are necessary for the present analysis and they are given in Appendix A. The boundary conditions (2.5)–(2.10) reduce at each order to their corresponding homogeneous forms. The bifurcation points, the bifurcating shapes from the base family and how these shapes are affected by varying the other relevant parameters of the problem are systematically determined in the following sections.

3.1. *Unperturbed bifurcation*

The unperturbed shapes are obtained by setting the variations of ΔP, ΔV and B equal to zero. Then, according to (3.7), $d_{\mathrm{I,O,P}}^{(0,1)} = 0$ and the first-order problem composed of (3.4)–(3.6) constitutes a homogeneous and linear eigenvalue problem with homogeneous boundary conditions. This problem has non-trivial solutions for specific values of the aspect ratio $\alpha^{(0,0)}$ which simultaneously define the locations of the bifurcation points from which the less symmetric bifurcating families emanate. The corresponding non-trivial solutions for the interface shapes and fluid pressure $(R_{\mathrm{I}}^{(1,0)}, R_{\mathrm{O}}^{(1,0)}, P_{\mathrm{F}}^{(1,0)})$ constitute the eigenvectors, which are also known as the null vectors of the linear differential operator defined by the left-hand side of (3.4)–(3.6). These solutions are of the form

$$R_{\mathrm{I}}^{(1,0)} = C_1 \cos\mu z + C_2 \sin\mu z + (1-t)^2 P_{\mathrm{F}}^{(1,0)}, \tag{3.8}$$

$$R_{\mathrm{O}}^{(1,0)} = C_3 \cos\delta z + C_4 \sin\delta z - P_{\mathrm{F}}^{(1,0)}, \tag{3.9}$$

where $P_{\mathrm{F}}^{(1,0)}$ is determined by the linearized volume constraint. The integration constants, C_i, are determined by the first-order boundary conditions, and they are non-trivial when the following characteristic equation in terms of $\alpha^{(0,0)}$ is satisfied:

$$\tan(\tfrac{1}{2}\mu)\tan(\tfrac{1}{2}\delta)[2\delta\xi^3\tan(\tfrac{1}{2}\mu) + 2\mu\tan(\tfrac{1}{2}\delta) - \mu\delta(1+\xi^3)] = 0, \tag{3.10}$$

where $\xi = 1-t$. Obviously, this equation has three types of roots which give rise to three types of eigenvectors as summarized in table 1. The corresponding families of solutions will be called the μ, δ and $\mu\delta$ families, and they group together shapes with

Shape family	Bifurcation points	Eigenfunctions
(μ)	$\alpha_n^{(0,0)} \equiv \dfrac{1}{\xi\mu_n} = \dfrac{1}{2n\pi\xi}$, $n = 1, 2, 3, \ldots$	$\begin{bmatrix} P_{\mathrm{F}}^{(1,0)} \\ R_{\mathrm{I}}^{(1,0)} \\ R_{\mathrm{O}}^{(1,0)} \end{bmatrix} = \begin{bmatrix} 0 \\ \sin(\mu_n z) \\ 0 \end{bmatrix}$
(δ)	$\alpha_n^{(0,0)} \equiv \dfrac{1}{\delta_n} = \dfrac{1}{2n\pi}$, $n = 1, 2, 3, \ldots$	$\begin{bmatrix} P_{\mathrm{F}}^{(1,0)} \\ R_{\mathrm{I}}^{(1,0)} \\ R_{\mathrm{O}}^{(1,0)} \end{bmatrix} = \begin{bmatrix} 0 \\ 0 \\ \sin(\delta_n z) \end{bmatrix}$
($\mu\delta$)	$2\delta_n \xi^3 \tan(\frac{1}{2}\mu_n) + 2\mu_n \tan(\frac{1}{2}\delta_n) - \mu_n \delta_n (1+\xi^3) = 0$, $n = 1, 2, 3, \ldots$	$\begin{bmatrix} P_{\mathrm{F}}^{(1,0)} \\ R_{\mathrm{I}}^{(1,0)} \\ R_{\mathrm{O}}^{(1,0)} \end{bmatrix} = \begin{bmatrix} 1 \\ \xi^2 \dfrac{[\sin\mu_n(1-\cos(\mu_n z)) - \sin(\mu_n z)(1-\cos\mu_n)]}{\sin\mu_n} \\ \dfrac{[\sin(\delta_n z)(1-\cos\delta_n) - \sin\delta_n(1-\cos(\delta_n z))]}{\sin\delta_n} \end{bmatrix}$

TABLE 1. Asymptotic results for unperturbed bifurcation from the base solution

perturbed inner, outer and both inner and outer interfaces, respectively. The shapes in both the μ and δ families are reflectively antisymmetric about the plane perpendicular to the axis of rotation at $z = \frac{1}{2}$; whereas the shapes of the $\mu\delta$ families are reflectively symmetric. By increasing the thickness of the meniscus, t, the bifurcation points for the μ and $\mu\delta$ families shift to higher values of the aspect ratio; whereas the δ bifurcation points are unaffected. For large values of the aspect ratio, α, the unperturbed annular shapes are stable. The highest value of α at which the annular shapes are neutrally stable occurs owing to the bifurcation of the first $\mu\delta$ family. A countable, but infinite number of new families emanate from the basic family as $\alpha \to 0$. Each successive family exhibits a more wavy shape than the previous one. This is similar to Rayleigh's (1879) results for the break-up of a liquid jet.

The evolution of the various shape families in the (α, ϵ)-plane is determined by calculating the corrections to the aspect ratio around each bifurcation point. We first define the amplitude of the perturbations for the $\mu\delta$ families, thus normalizing the eigenvectors, as follows:

$$\epsilon = \frac{1}{2}\left[\frac{\langle R_{\mathrm{I}}^{(1,0)}, R_{\mathrm{I}} - R_{\mathrm{I}}^{(0,0)}\rangle}{\langle R_{\mathrm{I}}^{(1,0)}, R_{\mathrm{I}}^{(1,0)}\rangle} + \frac{\langle R_{\mathrm{O}}^{(1,0)}, R_{\mathrm{O}} - R_{\mathrm{O}}^{(0,0)}\rangle}{\langle R_{\mathrm{O}}^{(1,0)}, R_{\mathrm{O}}^{(1,0)}\rangle}\right], \tag{3.11}$$

where the angle brackets denote the inner product between two functions $f(z)$ and $g(z)$ given by

$$\langle f, g\rangle = \int_0^1 f(z)\, g(z)\, \mathrm{d}z. \tag{3.12}$$

For the μ (δ) shape family the second (first) term in (3.11) is identically zero and the factor $\frac{1}{2}$ is dropped. The tangent of the angles between the different shape families and the base family are equal to $1/\alpha^{(1,0)}$. They are calculated so that the second-order inhomogeneous problem has a bounded solution. Equivalently, the null vector must be orthogonal to the right-hand side of (3.4)–(3.6) for $(n, m) = (2, 0)$, according to Fredholm's alternative (Ioos & Joseph 1980). The values of $\alpha^{(1,0)}$ are

$$\alpha^{(1,0)} = 0, \tag{3.13}$$

for either the μ or δ family irrespective of the meniscus thickness, and for the $\mu\delta$ family

$$\alpha^{(1,0)} = \alpha^{(0,0)} \frac{\xi^3[\gamma_1(\alpha^{(0,0)}\xi\delta_1 - 5) + \xi\zeta_1 - 4] - \gamma_2(\alpha^{(0,0)}\delta_2 - 5) - \zeta_2 + 4}{4\xi^2\gamma_1 + 4\gamma_2 - 8\alpha^{(0,0)}(\xi^3\beta_1 + \beta_2)}, \tag{3.14}$$

where $\gamma_i = 1 + \beta_i^2$, $\delta_i = 4\beta_i - \alpha^{(0,0)}$, $\zeta_1 = 2\alpha^{(0,0)}[(3\alpha^{(0,0)}\xi + 7)\beta_1 - \alpha^{(0,0)}]$,

$\zeta_2 = 2\alpha^{(0,0)}[(3\alpha^{(0,0)} + 7)\beta_2 - \alpha^{(0,0)}]$, $\beta_1 = \tan(\frac{1}{2}\mu)$, $\beta_2 = \tan(\frac{1}{2}\delta)$.

Therefore, the μ and δ families emanate perpendicularly to the base solution as do Rayleigh's modes for the break-up of a liquid jet. However, the $\mu\delta$ family forms an angle that depends on the dimensionless thickness and this bifurcation is called transcritical. In particular, the first and subsequently all the even $\mu\delta$ families have negative slopes and all the odd $\mu\delta$ families starting with the third have positive slopes for thickness values of $t = 0.1$. However, this slope for all $\mu\delta$ families except for the first can become positive and even infinite as the meniscus thickness increases. Since the first critical point always corresponds to a transcritical bifurcation, static menisci that belong to this branch with even smaller than critical α will be stable. Furthermore, the evolution of instabilities close to the first critical point, will be significantly different from that of a cylindrical jet and similar to the dynamics during break-up of a critically charged liquid drop (Tsamopoulos *et al.* 1985).

In order to characterize the μ and δ bifurcations it is necessary to calculate the next-order correction to the regular expansion for the aspect ratio. As previously, the solvability criterion for the third-order problem yields

$$\alpha^{(2,0)} = \frac{\alpha^{(0,0)}[\delta \sin\delta(3\xi^3 + 1) + 2(\cos\delta - 1)]}{4\xi^2[\delta \sin\delta(\xi^3 + 1) + 2(\cos\delta - 1)]}, \quad \text{for } \mu \text{ families,} \tag{3.15}$$

$$\alpha^{(2,0)} = \frac{\alpha^{(0,0)}[\mu \sin\mu(\xi^3 + 3) + 2\xi^3(\cos\mu - 1)]}{4[\mu \sin\mu(\xi^3 + 1) + 2\xi^3(\cos\mu - 1)]}, \quad \text{for } \delta \text{ families.} \tag{3.16}$$

These expressions yield positive values for $\alpha^{(2,0)}$ so that both μ and δ families bifurcate subcritically in aspect ratio. Second-order corrections to the aspect ratio for the $\mu\delta$ family reveal the existence of a limit point in these families and are given elsewhere (A. Poslinski, Ph.D. thesis, SUNY at Buffalo, in preparation). Additionally, the second-order corrections to meniscus shape for the μ family are

$$\begin{bmatrix} R_1^{(2,0)} \\ R_0^{(2,0)} \\ P_F^{(2,0)} \end{bmatrix} = \begin{bmatrix} \sin\mu z + \dfrac{\cos^2\mu z}{2\xi} - [(\delta \sin\delta + 2\cos\delta - 2)\cos\mu z + \delta \sin\delta\xi^3]/(D_1\xi) \\ \delta[\sin\delta(1 - \cos\delta z) - \sin\delta z(1 - \cos\delta)]/D_1 \\ -\delta \sin\delta/D_1 \end{bmatrix}, \tag{3.17}$$

where $D_1 = 2\delta \sin\delta(1 + \xi^3) + 4(\cos\delta - 1)$. For the δ family these corrections are

$$\begin{bmatrix} R_1^{(2,0)} \\ R_0^{(2,0)} \\ P_F^{(2,0)} \end{bmatrix} = \begin{bmatrix} \xi^2\mu[\sin\mu(1 - \cos\mu z) - \sin\mu z(1 - \cos\mu)/D_2 \\ \sin\delta z + \frac{1}{2}\cos^2\delta z - [(\mu \sin\mu + 2\cos\mu - 2)\xi^3\cos\delta z + \mu \sin\mu]/D_2 \\ \mu \sin\mu/D_2 \end{bmatrix}, \tag{3.18}$$

where $D_2 = 2\mu \sin\mu(1 + \xi^3) + 4\xi^3(\cos\mu - 1)$.

All the perturbation results agree very well with the numerical simulations given in §4 and are graphically represented there.

3.2. *Perturbed bifurcation*

Changes in the externally applied pressure, the liquid volume in the meniscus and the gravitational acceleration modify the solution structure and are calculated by expanding the field variables in terms of the above-mentioned parameters. To this end, ΔP, ΔV or B will be identified with γ in the Taylor series given by (3.3), and the resulting equations are of the form (3.4)–(3.6). Their solutions are regular away from the bifurcation points:

$$\Delta P \neq 0, \quad \begin{bmatrix} R_{\mathrm{I}}^{(0,1)} \\ R_{\mathrm{O}}^{(0,1)} \\ P_{\mathrm{F}}^{(0,1)} \end{bmatrix} = \frac{\Delta P^{(0,1)}}{D_3} \begin{bmatrix} \xi^2\mu(2\tan(\frac{1}{2}\delta)-\delta)(\tan(\frac{1}{2}\mu)\sin\mu z+\cos\mu z-1) \\ \xi^3\delta(2\tan(\frac{1}{2}\mu)-\mu)(\tan(\frac{1}{2}\delta)\sin\delta z+\cos\delta z-1) \\ \xi^3\delta(2\tan(\frac{1}{2}\mu)-\mu) \end{bmatrix}, \tag{3.19}$$

$$\Delta V \neq 0, \quad \begin{bmatrix} R_{\mathrm{I}}^{(0,1)} \\ R_{\mathrm{O}}^{(0,1)} \\ P_{\mathrm{F}}^{(0,1)} \end{bmatrix} = \frac{\Delta V^{(0,1)}}{2D_3} \begin{bmatrix} -\xi^2\mu\delta(\tan(\frac{1}{2}\mu)\sin\mu z+\cos\mu z-1) \\ \mu\delta(\tan(\frac{1}{2}\delta)\sin\delta z+\cos\delta z-1) \\ \mu\delta \end{bmatrix}, \tag{3.20}$$

$$B \neq 0, \quad \begin{bmatrix} R_{\mathrm{I}}^{(0,1)} \\ R_{\mathrm{O}}^{(0,1)} \\ P_{\mathrm{F}}^{(0,1)} \end{bmatrix} = \tfrac{1}{2}B^{(0,1)} \begin{bmatrix} \xi^2[\sin\mu z+\tan(\frac{1}{2}\mu)(1-\cos\mu z)-2z\tan(\frac{1}{2}\mu)]/\tan(\frac{1}{2}\mu) \\ -[\sin\delta z+\tan(\frac{1}{2}\delta)(1-\cos\delta z)-2z\tan(\frac{1}{2}\delta]/\tan(\frac{1}{2}\delta) \\ 1 \end{bmatrix}, \tag{3.21}$$

where

$$D_3 = 2\delta\xi^3\tan(\tfrac{1}{2}\mu)+2\mu\tan(\tfrac{1}{2}\delta)-\mu\delta(1+\xi^3). \tag{3.22}$$

However, the solutions for varying ΔP and ΔV become singular near the $\mu\delta$ bifurcation points, and the solutions for varying B become singular near the μ and δ bifurcation points. Therefore, near these respective points the singular behaviour must be resolved by rescaling the varying parameters with γ, and by developing the inner solution according to Reiss (1977) and Matkowsky & Reiss (1977). Equivalently, as Ungar & Brown (1982) have shown, the series (3.3) and Fredholm's alternative can be used to calculate the dependence of the varying parameters on γ. The latter technique avoids the rescaling procedure and provides directly inner solutions which are bounded. The development of singularities close to certain bifurcation points indicates that the solution varies significantly there. Indeed, the emanating solution families split and develop limit points. Furthermore, even when the solutions remain regular, the bifurcation points themselves shift to different values of the aspect ratio. Detailed analysis of all these possibilities is given in the following four subsections.

3.2.1. *Variation of ΔP near the $\mu\delta$ bifurcation points*

If only variations in the externally applied pressure are allowed, the right-hand side of the first-order equations (3.4)–(3.6) become $(d_{\mathrm{I}}^{(0,1)}, d_{\mathrm{O}}^{(0,1)}, d_P^{(0,1)}) = (-\delta^2\Delta P^{(0,1)}, 0, 0)$. Since the homogeneous solution to these equations, given in table 1, is simultaneously the null vector of the differential operator, the non-homogeneous solution is bounded if Fredholm's alternative is satisfied at $\alpha = \alpha^{(0,0)}$, i.e.

$$\langle R_{\mathrm{I}}^{(1,0)}, -\delta^2\Delta P^{(0,1)}\rangle = 0. \tag{3.23}$$

Equation (3.23) requires that $\Delta P^{(0,1)} = 0$, making the first-order perturbed problem homogeneous with a general solution determined up to an amplitude, K:

$$(R_{\mathrm{I}}^{(0,1)}, R_{\mathrm{O}}^{(0,1)}, R_{\mathrm{F}}^{(0,1)}) = K(R_{\mathrm{I}}^{(1,0)}, R_{\mathrm{O}}^{(1,0)}, P_{\mathrm{F}}^{(1,0)}). \tag{3.24}$$

In order to determine K, the solvability criterion for the second-order problem is invoked and yields

$$K^2 I_2 + K\alpha^{(0,1)} I_1 + \Delta P^{(0,2)} I_0 = 0, \tag{3.25}$$

where the expressions I_i result from the evaluation of the inner product and are given in Appendix B. Equation (3.25) is quadratic in K which then depends on the first correction to aspect ratio and the imposed external pressure

$$\Delta P = \gamma^2 \Delta P^{(0,2)}. \tag{3.26}$$

Without loss of generality $\Delta P^{(0,2)} = \pm 1$ corresponding to inflation or deflation of the meniscus. Therefore, the imposed pressure, ΔP, scales with the square of the peturbation parameter, γ, and setting the distance, $\alpha^{(0,1)}$, from the $\mu\delta$ bifurcation point, determines the amplitude, K, through (3.25). For a given pair $(\alpha^{(0,1)}, \gamma)$ there may be either two, one or no solutions for K. Of special interest is the case of a double root, since it provides the loci of the limit points formed by the broken bifurcating families to be $\alpha^{(0,0)} + \gamma\alpha^{(0,1)}$, where

$$\alpha^{(0,1)} = \pm\left(\frac{4I_0 I_2 \Delta P^{(0,2)}}{I_1^2}\right)^{\frac{1}{2}}. \tag{3.27}$$

The two different signs of $\Delta P^{(0,2)}$ lead to drastically different splitting of every bifurcation point as shown in §4.2. In general, one set of limit points exists above the base solution and one below. Sample numerical values of the limit points are given in §4.2 and further details can be found elsewhere (A. Poslinski, Ph.D. thesis in preparation).

3.2.2. *Variation of ΔV near the $\mu\delta$ bifurcation points*

In a similar way, when $(d_{\mathrm{I}}^{(0,1)}, d_{\mathrm{O}}^{(0,1)}, d_{\mathrm{P}}^{(0,1)}) = (\frac{1}{2}\Delta V^{(0,1)}, 0, 0)$ Fredholm's alternative requires that $\Delta V^{(0,1)} = 0$. Then the solution of the first-order problem is given by (3.24). The solvability criterion of the second-order problem yields the same quadratic equation for K except that here $I_0 = \frac{1}{2}$. From the expansion (3.3),

$$\Delta V = V - t(2-t) = \gamma^2 \Delta V^{(0,2)}. \tag{3.28}$$

One can now set $\Delta V^{(0,2)} = \pm 1$ indicating an increase or decrease of the annular fluid volume. Once again, the values of $\alpha^{(0,1)}$ that result in double roots for K are the limit points in the broken bifurcation families, (see also §4.3).

3.2.3. *Variation of B near the μ or δ bifurcation points*

When only variations in gravity are considered the homogeneous terms in (3.4)–(3.6) become $(d_{\mathrm{I}}^{(0,1)}, d_{\mathrm{O}}^{(0,1)}, d_{\mathrm{P}}^{(0,1)}) = (-\delta^2 B^{(0,1)} z, \delta^2 B^{(0,1)} z, 0)$. The solvability criterion requires that $B^{(0,1)} = 0$, so that the solution to the first-order problem remains the same as in §§3.2.1 and 3.2.2. However, the second-order solution becomes bounded when an equation of the form (3.25) is satisfied with $I_2 = 0$. As noted by Matkowsky & Reiss (1977), a unique solution for K in the inner problem is unable to match all three outer solutions which exist in subcritical bifurcations for

Shape family	Varying parameter	
(μ)	Pressure	$\alpha^{(0,1)} = [2\tan(\frac{1}{2}\delta) - \delta]\Delta P^{(0,1)}/D_4$,
	Volume	$\alpha^{(0,1)} = -\delta\Delta V^{(0,1)}/(2D_4)$,
(δ)	Pressure	$\alpha^{(0,1)} = [2\tan(\frac{1}{2}\mu) - \mu]\xi^3\Delta P^{(0,1)}/D_5$,
	Volume	$\alpha^{(0,1)} = \mu\Delta V^{(0,1)}/2D_5$),
($\mu\delta$)	Gravity	$\alpha^{(0,1)} = 0$.

where $D_4 = \mu[2\tan(\frac{1}{2}\delta) - \delta(1+\xi^3)]$,
and $D_5 = \delta[2\xi^3\tan(\frac{1}{2}\mu) - \mu(1+\xi^3)]$.

TABLE 2. Coefficients for the shift of unbroken bifurcation points

some parameter range. Consequently, this inner solution has to be dropped by setting

$$\alpha^{(0,1)} = B^{(0,2)} = 0. \tag{3.29}$$

The solution to the second-order problem reduces to

$$(R_{\mathrm{I}}^{(0,2)}, R_{\mathrm{O}}^{(0,2)}, P_{\mathrm{F}}^{(0,2)}) = K^2(R_{\mathrm{I}}^{(2,0)}, R_{\mathrm{O}}^{(2,0)}, P_{\mathrm{F}}^{(2,0)}), \tag{3.30}$$

where the terms on the right-hand side are given by (3.17) and (3.18). In order to determine K, Fredholm's alternative is invoked for the third-order problem to yield

$$K^3 I_5 + K\alpha^{(0,2)} I_4 + B^{(0,3)} I_3 = 0, \tag{3.31}$$

where I_i again result from the evaluation of the inner product and are given in Appendix B. According to (3.31), one, two or three values of K may correspond to specified values of $B^{(0,3)}$ and $\alpha^{(0,2)}$. Without loss of generality one can set $B^{(0,3)} = 1$ and deduce from (3.3) that variations in the gravitational Bond number should scale with the third power of γ. Furthermore, introducing the effects of gravity splits the subcritical μ and δ bifurcating families into a continuous family and one with a limit point for specific values of the aspect ratio. Setting the discriminant of (3.31) to zero determines the loci of these limit points as $\alpha = \alpha^{(0,0)} + \gamma^2\alpha^{(0,2)}$, where

$$\alpha^{(0,2)} = \left[\frac{27\xi^6\alpha^{(2,0)}}{4\delta^5\alpha^{(0,0)}}\right]^{\frac{1}{3}}, \tag{3.32}$$

for the μ families, and

$$\alpha^{(0,2)} = \left[\frac{27\alpha^{(2,0)}}{4\delta^5\alpha^{(0,0)}}\right]^{\frac{1}{3}}, \tag{3.33}$$

for the δ families. Both (3.32) and (3.33) yield $\alpha^{(0,2)} > 0$ so that the limit points arise at higher values in aspect ratio than the corresponding bifurcation points. The position of the single set of limit points with respect to the base solution depends now on the sign of the double root of K derived from (3.31). The perturbed bifurcation diagram is given in §4.

3.2.4. *Shifting of unbroken bifurcation points*

The regular perturbation solutions (3.19)–(3.21) remain bounded when pressure or volume variations are considered close to the μ and δ bifurcation points and when gravity variations are considered close to the $\mu\delta$ bifurcation points. Thus, under

these variations the bifurcation points remain unbroken, but arise at modified values of α. According to Reiss (1977) this shifting of the bifurcation points is obtained by considering the two-variable expansion (3.3) up to order $\epsilon^1\gamma^1$. Since the three lower-order problems $(\epsilon^0\gamma^0, \epsilon^1\gamma^0, \epsilon^0\gamma^1)$ have already been considered this new term can be calculated readily. Consequently, the bifurcation points shift from their original values $\alpha^{(0,0)}$ as follows:

$$\alpha = \alpha^{(0,0)} + \epsilon\alpha^{(1,0)} + \gamma\alpha^{(0,1)}. \tag{3.34}$$

Table 2 lists the values of $\alpha^{(0,1)}$ for each unbroken bifurcation point. Given that both μ and δ bifurcating families are subcritical, small positive pressure increases cause a shift to higher values of the aspect ratio. Moreover, small volume increases shift these families away from each other. Finally, the $\mu\delta$ bifurcation points are not shifted when gravity varies, since $\alpha^{(0,1)} = 0$.

3.3. *Non axisymmetric bifurcations*

The possibility of bifurcations to non-axisymmetric shape families, under the restriction that the liquid meniscus remains vertical is examined next. Substituting the expansion (3.3) into the governing equations (2.1)–(2.4) yields the following set of linear partial differential equations at first order in ϵ:

$$\frac{\partial^2 R_{\mathrm{I}}^{(1,0)}}{\partial z^2} + \mu^2 \frac{\partial^2 R_{\mathrm{I}}^{(1,0)}}{\partial \theta^2} + \mu^2 R_{\mathrm{I}}^{(1,0)} - \delta^2 P_{\mathrm{F}}^{(1,0)} = 0, \tag{3.35}$$

$$\frac{\partial^2 R_{\mathrm{O}}^{(1,0)}}{\partial z^2} + \delta^2 \frac{\partial^2 R_{\mathrm{O}}^{(1,0)}}{\partial \theta^2} + \delta^2 R_{\mathrm{O}}^{(1,0)} + \delta^2 P_{\mathrm{F}}^{(1,0)} = 0, \tag{3.36}$$

$$\int_0^{2\pi} \int_{-\frac{1}{2}}^{\frac{1}{2}} (R_{\mathrm{O}}^{(1,0)} - \xi R_{\mathrm{I}}^{(1,0)})\, \mathrm{d}z\, \mathrm{d}\theta = 0, \tag{3.37}$$

where the coordinate system has been shifted to the centre of the midplane between the two horizontal solid surfaces for convenience. The solution of this set of equations subject to the homogeneous boundary conditions derived from (2.5)–(2.10) is given by

$$R_{\mathrm{I}}^{(1,0)}(z,\theta) = [C_1 \cos(\beta_3 z) + C_2 \sin(\beta_3 z)] \cos k\theta, \tag{3.38}$$

$$R_{\mathrm{O}}^{(1,0)}(z,\theta) = [C_3 \cos(\beta_4 z) + C_4 \sin(\beta_4 z)] \cos k\theta, \tag{3.39}$$

$$P_{\mathrm{F}}^{(1,0)} = 0, \tag{3.40}$$

where k is any non-negative integer, $\beta_3 = \mu(1-k^2)^{\frac{1}{2}}$ and $\beta_4 = \delta(1-k^2)^{\frac{1}{2}}$ and C_i are integration constants. A non-trivial solution is derived only when $\alpha^{(0,0)}$ is such that the following characteristic equation is satisfied:

$$\sin(\beta_3) \cos(\beta_3) \sin(\beta_4) \cos(\beta_4) = 0. \tag{3.41}$$

For $k = 0$, equations (3.38)–(3.40) reduce to the μ and δ axisymmetric bifurcating families. For $k = 1$, the same equations predict a uniform translation of the meniscus in a plane containing the z-axis. For $k > 1$, no bifurcating solutions exist, as should be expected by analogy with the cylindrical jet. However, it is expected that if the meniscus is tilted with respect to the gravitational field, stable non-axisymmetric shape families will indeed arise. This possibility is not explored further.

4. Numerical results on equilibrium shapes and stability

Since the non-axisymmetric analysis in §3.3 revealed that no such shape families emanate, the numerical simulation is focused on determining axisymmetric families for large deformations. A finite-element algorithm is used to calculate equilibrium shapes as well as bifurcation and limit points. The inner and outer liquid/gas interfaces are represented in terms of Lagrange quadratic basis functions $\{\phi^i(z)\}$:

$$R_{\mathrm{I}}(z) = \sum_{i=1}^{N} x_i \phi^i(z), \quad R_{\mathrm{O}}(z) = \sum_{i=N+1}^{2N} x_i \phi^i(z), \tag{4.1}$$

where the coefficients $\{x_i\}$ are determined so that the weighted equations (2.1) and (2.2) according to Galerkin's methodology are zero (Strang & Fix 1973). The fluid pressure is the final unknown and is determined from the constraint that the volume of the meniscus remains constant. This procedure yields $2N+1$ algebraic equations

$$\boldsymbol{R}(\boldsymbol{x}) = \boldsymbol{0}, \tag{4.2}$$

for the interface shapes and fluid pressure, where $\boldsymbol{x} = (x_1, x_2, \ldots, x_{2N}, P_{\mathrm{F}})$. Since the Lagrangian interpolation does not guarantee intra-element continuity of the derivatives in the finite-element representation, care must be taken so that second-order derivatives do not arise in the weak formulation. The algebraic set (4.2) is solved by Newton's method which starts from an initial guess $\boldsymbol{x}^{(0)}$ and calculates successive approximations to the solution as

$$\boldsymbol{x}^{(k+1)} = \boldsymbol{x}^{(k)} - \boldsymbol{J}^{-1}\boldsymbol{R}(\boldsymbol{x}^{(k)}), \tag{4.3}$$

where the Jacobian matrix, $\boldsymbol{J}$, is analytically calculated and is symmetric. Furthermore, $\boldsymbol{J}$ is sparse and is composed of a banded part of length $2N$ and bandwidth five, and a final dense row and column due to the volume constraint. The efficient routine ARROW, developed by Thomas & Brown (1987) was used for the inversion of $\boldsymbol{J}$. Typically five iterations were sufficient to achieve a solution with error less than 10^{-8}. The method was tested for accuracy by varying the number of elements. Such variations from 100 to 500 elements resulted in values for the bifurcation and limit points that were different by less than 0.5%. Consequently, 250 elements were used in order to achieve an optimum between numerical error and computational cost.

The numerical procedure closely follows the work of Ungar & Brown (1982) and the techniques of Keller (1977) for efficient calculations around limit points, and of Abbott (1978) for directly locating limit and bifurcating points with variations in the parameters of the problem. For this reason and for brevity, further details have been omitted in the present work.

The stability of a particular shape family to steady perturbations is related directly to its location in the bifurcation diagram and its connectivity with the base family. According to the theorem of exchange of stability at double points, the stability of solution families must change at each limit point and at each bifurcation point, and only at such points (Ioos & Joseph 1980). The only requirement is that the base family is known to be stable for some parameter values. Calculations of the eigenvalues for a solution family are only necessary when no shapes are known to be stable. However, selective calculations of eigenvalues have been carried out and have merely confirmed the results of bifurcation theory. The following sections §§4.1–4.4 present numerical results for the unperturbed and perturbed problems, respectively.

Bifurcating shape family	Exact value of α	Finite-element calculation
$\mu\delta$	0.33742	0.3374
μ	0.17684	0.1768
δ	0.15915	0.1591
$\mu\delta$	0.12088	0.1209
$\mu\delta$	0.10822	0.1082

TABLE 3. Locations of bifurcation points for $t = 0.1$

4.1. *Unperturbed annular menisci*

The annular base family is the solution for all aspect ratios and meniscus thicknesses, when $\Delta P = \Delta V = B = 0$. This family is stable for large values of the aspect ratio and up to the first transcritical bifurcation to a $\mu\delta$ family. One of the tests for accuracy of the finite-element approximations is performed by comparing the numerical results for the first five bifurcation points to the asymptotic results given in §3.1. As shown in table 3, the agreement is excellent.

The families of static shapes evolving from the first five bifurcation points are presented in figure 2 for $t = 0.1$. The slope of the first bifurcating family is numerically calculated to be -0.784 which compares well with the analytical value of $1/\alpha^{(1,0)} = -0.781$. Therefore, its upper branch continues to lower values of the aspect ratio and is stable up to the value $\alpha = 0.3017$ where a limit point arises. Subsequently, this branch turns to higher values of aspect ratio and the calculated equilibrium shapes become unstable. The lower branch of the same family directly develops towards larger values of aspect ratio and is composed of unstable equilibrium shapes.

The next shape families that bifurcate as α decreases belong to the μ and δ types, and they evolve subcritically as predicted by the asymptotic analysis. In order to observe this, an expanded view close to the bifurcation points is shown in figure 3. All bifurcating families except for the upper segment of the first one and before the limit point are unstable. Infinite bifurcation points arise and occur closer together as the aspect ratio approaches zero. The analytical solutions were carried out up to the calculation of the slope of the $\mu\delta$ shape families and up to the calculation of the curvature of the μ and δ shape families. They are shown in figures 2 and 3 and the finite-element calculations establish their range of validity. As indicated by the dotted lines, linear theory predicts very well the slopes of the $\mu\delta$ bifurcating families. In addition, for deformed shapes in the μ and δ families which are characterized by $\epsilon \leqslant 0.1$ the analytically and numerically obtained bifurcation curves coincide.

Figure 4 shows the variation of the first three bifurcation points for each type of shape family with meniscus thickness. With increasing thickness, both the μ and $\mu\delta$ bifurcation points shift to higher values of the aspect ratio, thus decreasing the range of stable shapes. This destabilization of the meniscus is because the larger thickness leads to a decrease in the inner radius and makes the inner surface more readily susceptible to capillary instability. However, the δ bifurcation points remain constant as predicted from the asymptotic analysis. This should be expected since the corresponding shapes have only their outer interfaces perturbed which are not affected by changes in thickness. The first δ bifurcating family arises at $\alpha = 1/2\pi$ and is the analogue of the first unstable mode for the break-up of a liquid jet. Indeed, as

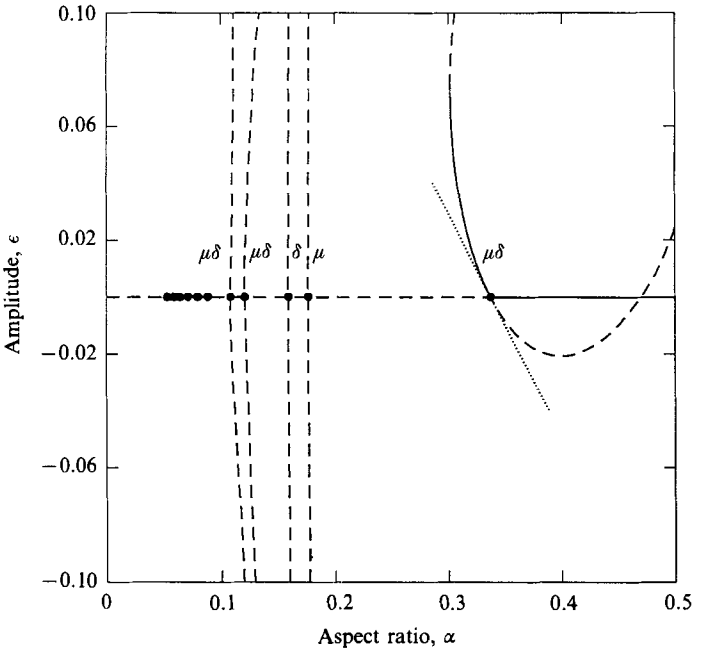

FIGURE 2. Unbroken bifurcation diagram ($\Delta P = \Delta V = B = 0, t = 0.1$): ——, stable solution families; – – –, unstable solution families; · · ·, asymptotic result; ●, bifurcation points.

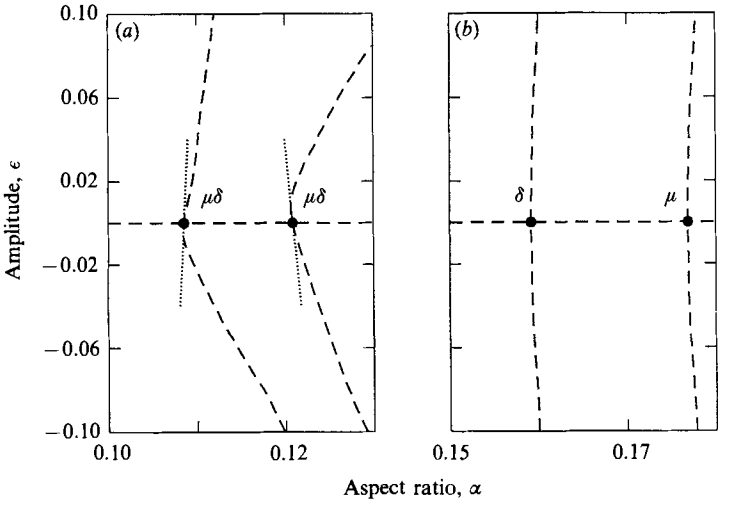

FIGURE 3. Expanded view of (*a*) the second and third $\mu\delta$ bifurcation families, and (*b*) the first δ and μ families: – – –, unstable solution families; · · ·, asymptotic result; ●, bifurcation points.

the meniscus thickness increases and reaches 1, the μ and $\mu\delta$ bifurcation points approach asymptotically large values in aspect ratio. However, the δ bifurcation points do not depend on t and are the ones that determine the stability of the liquid cylinder at the limit of $t = 1$. Thus, the Rayleigh modes are recovered. For the other limiting value of the thickness, $t \to 0$, the values of the μ and δ bifurcation points approach each other. Obviously, as the thickness is varied, there exist values of α for

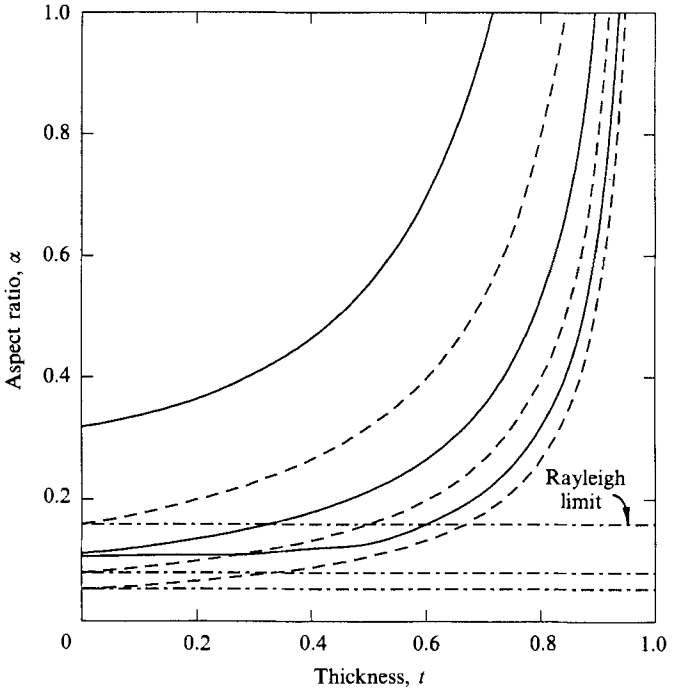

FIGURE 4. Dependence of the first three bifurcation points for each type of shape family on the thickness of the annular meniscus: ——, $\mu\delta$ shape family; – – –, μ shape family; —·—, δ shape family.

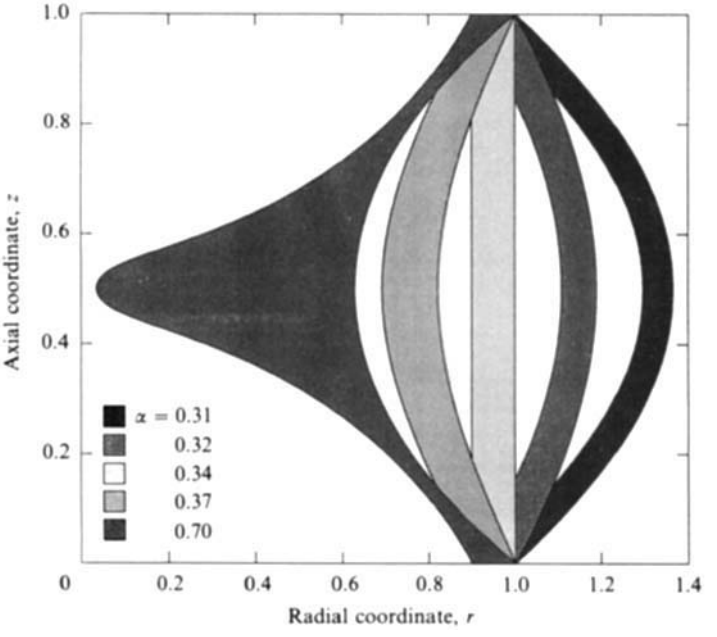

FIGURE 5. Meniscus shapes on the first bifurcating family; $\alpha = 0.34$ is the base solution and $t = 0.1$.

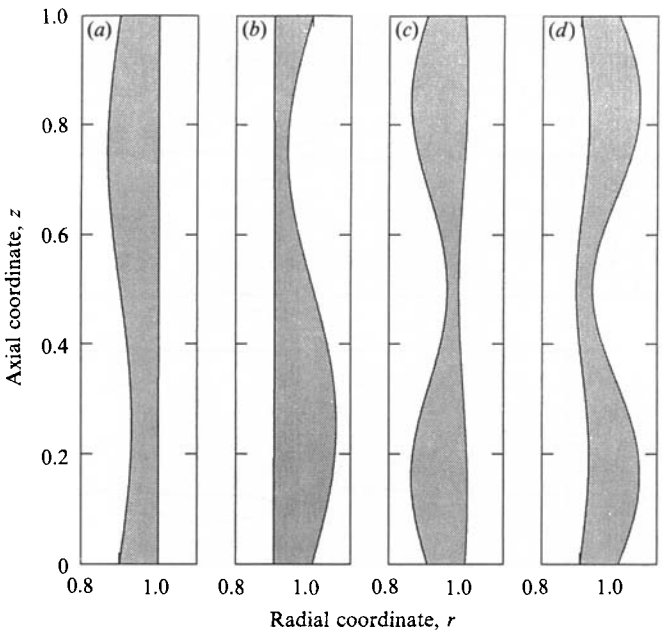

FIGURE 6. Meniscus shapes on the subsequently bifurcating families: (*a*) μ family, $\alpha = 0.18$; (*b*) δ family, $\alpha = 0.16$; (*c*) second $\mu\delta$ family, $\alpha = 0.12$; (*d*) third $\mu\delta$ family, $\alpha = 0.11$. Only upper-branch shapes are shown for $t = 0.1$.

which higher-order bifurcation points arise, whenever the μ or $\mu\delta$ loci of bifurcation points intersect the δ ones or each other. Only the first $\mu\delta$ shape family is an exception to these observations and does not pair with any other family.

Figure 5 illustrates the meniscus segments associated with the first bifurcating family for $t = 0.1$ and various values of α. The upper branch of the first $\mu\delta$ family resembles inflation. It is this shape with the increased inner radius that renders menisci in this family stable. Typical shapes for the second to the fifth families are shown in figure 6. The shapes of μ and δ bifurcating families appear sinusoidal in the inner and outer interfaces, respectively. The second and third $\mu\delta$ families have both the inner and outer interfaces sinusoidal with half the wavelength and more deformation of the inner and outer interfaces, respectively. This behaviour is consistent with the shifting of the loci of the $\mu\delta$ bifurcation points as thickness varies.

4.2. *Changes in externally applied pressure*

Increasing or decreasing the additional pressure, ΔP, applied to the inner interface causes the meniscus to inflate or deflate, respectively. This variation in applied pressure preserves the character of the reflectively symmetric shape families. Therefore, it should provide an easy transition from the slightly deformed annular shapes to inflated ones by transforming the transcritical $\mu\delta$ bifurcations to smooth curves. Indeed, as shown in figure 7(*a*) for $\Delta P > 0$ and in figure 7(*b*) for $\Delta P < 0$ at $t = 0.1$ the $\mu\delta$ bifurcation points are ruptured. Under inflating conditions two curves with finite slope are created close to the first bifurcation point. Under deflating conditions the two curves split giving rise to two limit points. The remaining $\mu\delta$ families are broken similarly, and in accordance with the prediction of (3.27).

The limit points obtained upon breaking the first three $\mu\delta$ shape families for

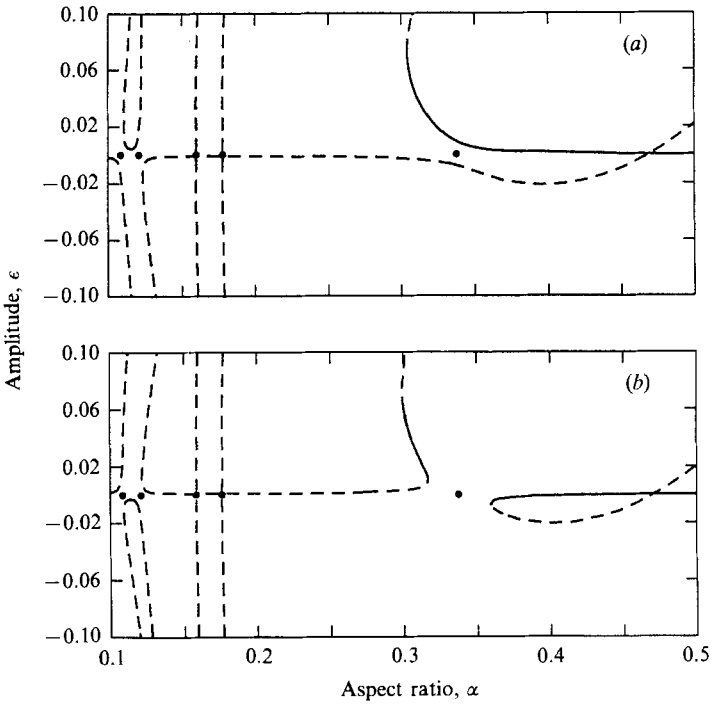

FIGURE 7. Broken bifurcation diagram due to a pressure variations with $t = 0.1$. (*a*) $\Delta P = 0.01$, (*b*) $\Delta P = -0.01$. ——, stable solution families; – – –, unstable solution families; ●, bifurcation points.

Pressure variation	Asymptotic value	Numerical value	Asymptotic value	Numerical value	Corresponding bifurcation point
−0.01	0.359	0.359	0.316	0.316	0.3374
+0.01		No limit points arise			0.3374
−0.01		No limit points arise			0.1209
+0.01	0.122	0.123	0.119	—	0.1209
−0.01		No limit points arise			0.1082
+0.01	0.109	0.111	0.107	—	0.1082

TABLE 4. Limit points created by perturbations in pressure

$t = 0.1$ are listed in table 4. The agreement between numerical and asymptotic results is very good. However, at the higher-order instabilities the bifurcating branches are very close to each other and the shapes are highly distorted making the numerical detection of the limit points increasingly difficult.

The region of stable inflated shapes starts again at large α and terminates at a limit point in α which develops from the limit point of the unbroken curve. This limit point shifts to larger aspect ratios as ΔP increases, see figure 8. The region of stable deflated shapes starts similarly from large aspect ratios, but terminates at limit points in α which are created by the breaking of the bifurcation point. For deflating conditions and $-0.1 < \Delta P < 0$ there is a small range of aspect ratios less than the first critical point for which stable shapes are predicted. They comprise families which are disconnected from the other stable deflating families. The evolution of the static family branches is clearly shown in figure 8 for varying pressures.

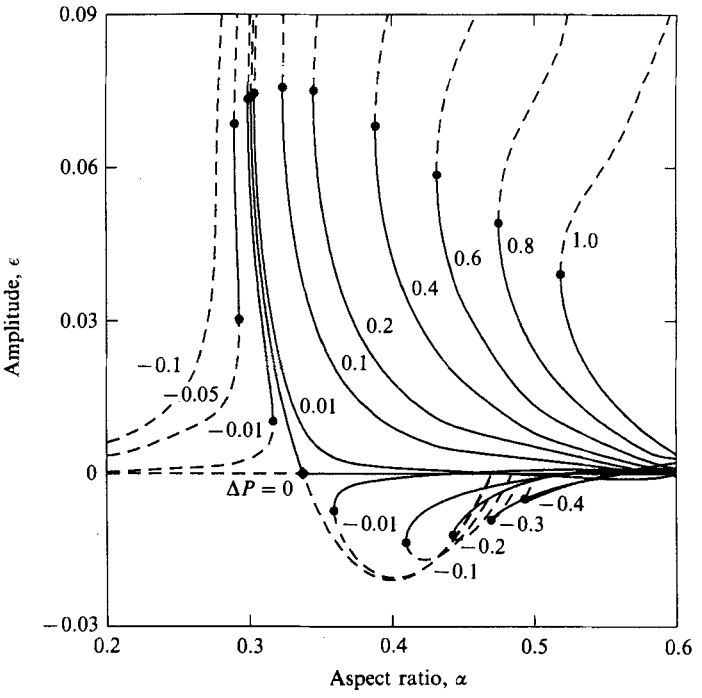

FIGURE 8. Dependence of the base and the first bifurcating family on the externally applied pressure, ΔP, for $t = 0.1$: ——, stable solutions; – – –, unstable solutions; ●, limit points; ◆, bifurcation points.

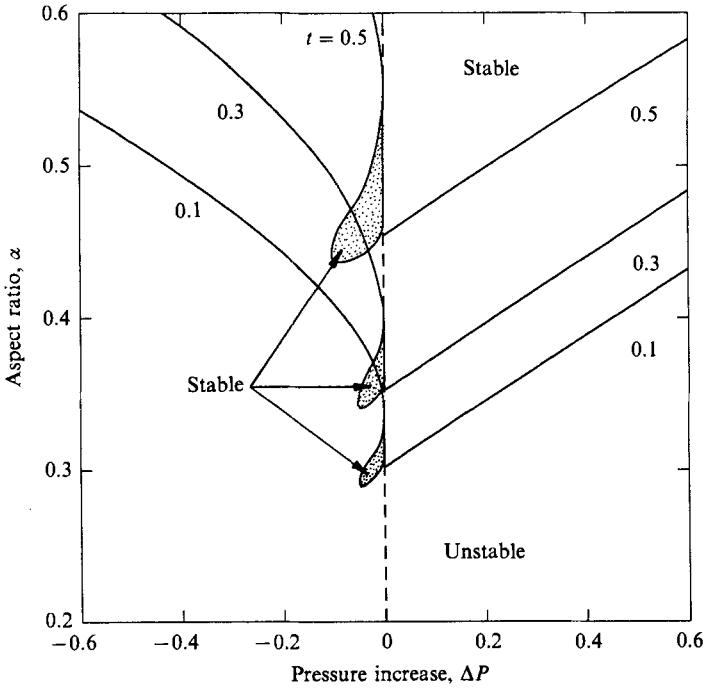

FIGURE 9. Stable and unstable operating regions for various applied pressures with the meniscus thickness as a parameter.

Bifurcation point	Pressure variation	Shifted value
0.177	+0.1	0.186
0.177	−0.1	0.168
0.159	+0.1	0.165
0.159	−0.1	0.153

TABLE 5. Shifting of bifurcation points for $t = 0.1$

Figure 9 shows the regions of stable shapes for inflation and deflation at various values of the meniscus thickness. As thickness increases and applied pressure increases or decreases, the range of aspect ratios with stable shapes decreases. The limit points in the lower branch for $t = 0.1$ and small ΔP are calculated from (3.27), and compare well with values calculated numerically. The above-mentioned additional stable shapes under deflating conditions appear in this figure as islands separated from the rest of the stable region. The meniscus shapes associated with the broken branches are similar to the corresponding unperturbed branch. The μ and δ bifurcation points do not break with variation of pressure owing to the reflectively antisymmetric shapes in the emanating families. Table 5 shows that they both shift to higher values of the aspect ratio with increasing ΔP, and that the numerical results are identical to the asymptotic ones predicted from (3.34) to the reported accuracy.

4.3. *Changes in meniscus volume*

Variations in the liquid volume preserve the character of the reflectively symmetric shape families also. Therefore, only the bifurcation points between what were the annular and $\mu\delta$ shape families break to create limit points. Decreases in volume draw the fluid/gas interfaces towards each other; whereas volume increases push these interfaces apart. Figures 10(*a*) and 10(*b*) show the modified bifurcation diagram for $t = 0.1$ for volume increase and decrease, respectively. When $\Delta V > 0$ the first bifurcation point splits, giving rise to two limit points. These newly created limit points move rapidly away from each other as the volume increases because of the predicted quadratic dependence of ΔV on α close to these limit points. When $\Delta V < 0$ two curves with finite slope exist around the limit point. The same two possibilities arise in the other $\mu\delta$ bifurcation points. In general, increases in volume produce qualitatively similar results to decreases in pressure and vice versa. The physical reason behind this result is that volume increases or pressure decreases lead to a decrease of the inner radius of the annulus; therefore, they make it more readily susceptible to capillary-driven instabilities.

The limit points obtained upon breaking the first three $\mu\delta$ families for $t = 0.1$ are listed in table 6 and show excellent agreement between the asymptotic predictions and numerical calculations. The region of stable shapes, having slightly larger or smaller volume than the volume of the annular shape, spans from large aspect ratios down to a limit point that depends on the thickness and volume variations. Again, for $0 < \Delta V < 0.2$ there is a small range of aspect ratios less than the first bifurcation point for which stable shapes are predicted.

Figure 11 indicates the limits of achievable static shapes given the thickness and volume of the meniscus. If the volume deviates from the annulus or the thickness increases, the stable operation limits decrease. The disconnected stable families appear again as isolated islands. In addition, stable shapes with volume decreases are

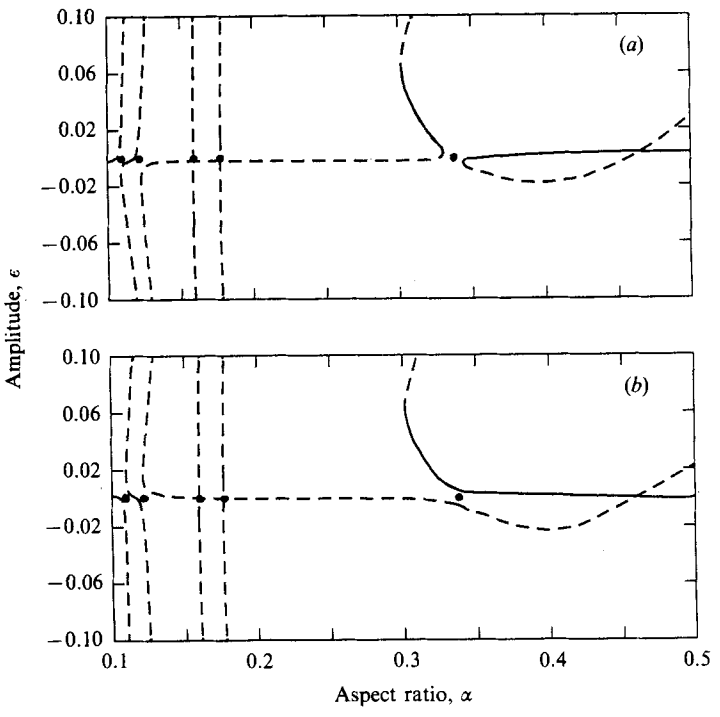

FIGURE 10. Broken bifurcation diagram due to meniscus volume variations with $t = 0.1$. (*a*) $\Delta V = 0.01$, (*b*) $\Delta V = -0.01$; ——, stable solution families; – – –, unstable solution families; ●, bifurcation points.

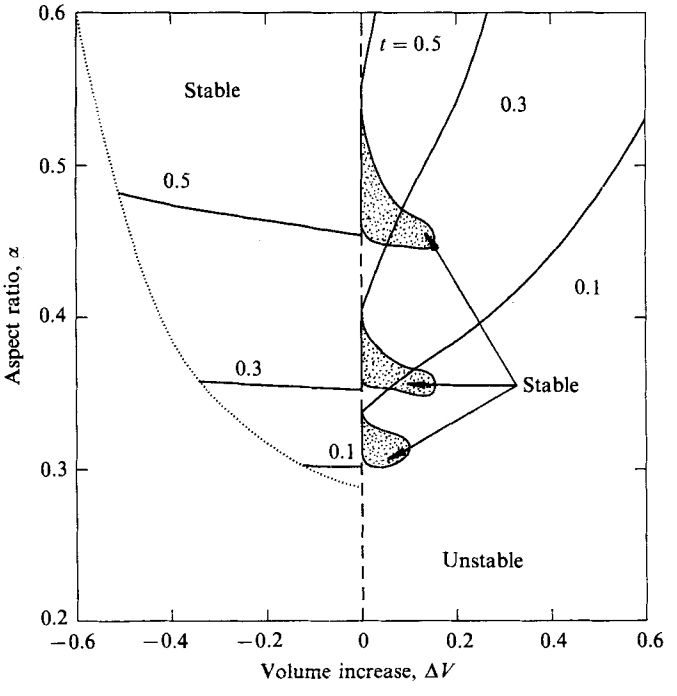

FIGURE 11. Stable and unstable operating regions for various meniscus volumes with the meniscus thickness as a parameter. The dotted line represents volume decreases that result in touching interfaces.

Volume variation	Asymptotic value	Numerical value	Asymptotic value	Numerical value	Corresponding bifurcation point
0.01	0.340	0.344	0.332	0.332	0.3374
−0.01		No limit points arise			0.3374
0.01	0.122	0.123	0.120	—	0.1209
−0.01		No limit points arise			0.1209
0.01		No limit points arise			0.1082
−0.01	0.109	0.110	0.107	—	0.1082

TABLE 6. Limit points created by perturbations in volume

Bifurcation point	Volume variation	Shifted value
0.177	+0.1	0.181
0.177	−0.1	0.173
0.159	+0.1	0.154
0.159	−0.1	0.164

TABLE 7. Shifting of bifurcation points for $t = 0.1$

limited by the dotted curve signifying that the inner and outer interfaces touch each other.

Table 7 shows that the unbroken bifurcation points shift towards each other when volume decreases, whereas they shift away from each other when volume increases in accordance with the predictions of (3.34) and table 2. Typical fluid menisci with a decrease or increase in fluid volume are shown in figures 12(*a*) and 12(*b*), respectively.

4.4. *Changes in gravitational Bond number*

The gravitational force pulls the meniscus towards the $z = 0$ plane. Figure 13 shows the perturbed bifurcation diagram with $t = 0.1$ and a positive gravitational Bond number, $B = 0.01$. The qualitative behaviour was predicted by the asymptotic analysis in §3.2. The reflectively antisymmetric shape families are broken whereas the reflectively symmetric remain unbroken and the corresponding bifurcation points are unshifted. A slight change of the first bifurcation point from $\alpha^{(0)} = 0.337$ to 0.338 is attributed to the translation of the base families as gravity increases from zero. In particular, the first bifurcating shape family is unaffected by changes in B.

Table 8 lists the limit points created by breaking the μ and δ bifurcation points. The asymptotic and numerical values are identical up to three digits of accuracy. Since the first bifurcation point is not broken when gravity increases from zero, the static shapes lose stability at the limit point on the upper branch of this bifurcating family.

Finally, several numerical simulations have been performed by simultaneously varying two or more of the parameters. For example, figure 12(*c*) shows a stable meniscus shape at $B = 0.5$ and $\Delta P = \Delta V = 0$ and figure 12(*d*) shows a stable meniscus shape obtained at $\Delta P = 0.4$, $\Delta V = 0.2$, $B = 0.5$, both at $t = 0.1$ and $\alpha = 0.5$. The results are consistent with the previous discussion. Finally, figure 14 indicates the range of values of α for which stable shapes can be achieved for various

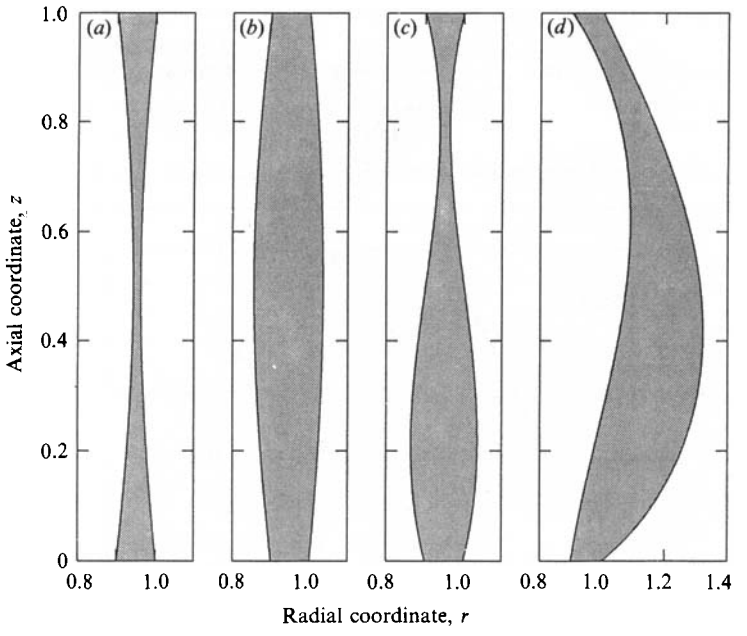

FIGURE 12. Meniscus shapes with $\alpha = 0.5$, $t = 0.1$ and varying parameters: (*a*) $\Delta V = -0.1, B = \Delta P = 0$; (*b*) $\Delta V = 0.1, B = \Delta P = 0$; (*c*) $B = 0.5, \Delta V = \Delta P = 0$; (*d*) $\Delta P = 0.4, \Delta V = 0.2, B = 0.5$.

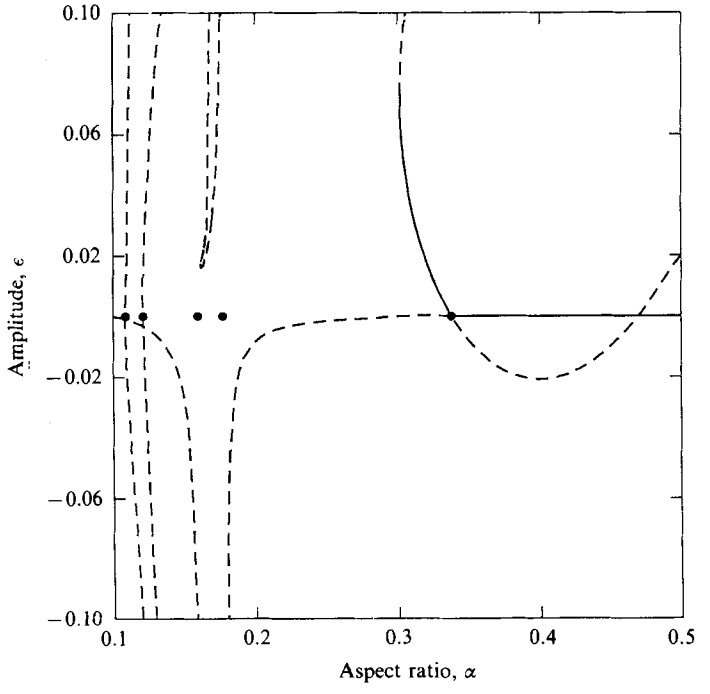

FIGURE 13. Broken bifurcation diagram due to gravitational force with $t = 0.1$ and $B = 0.01$: ——, stable solution families; – – –, unstable solution families; ●, bifurcation points.

Gravity variation	Limit point	Corresponding bifurcation point
0.01	0.180	0.177
0.01	0.163	0.159

TABLE 8. Limit points created by perturbations in gravity

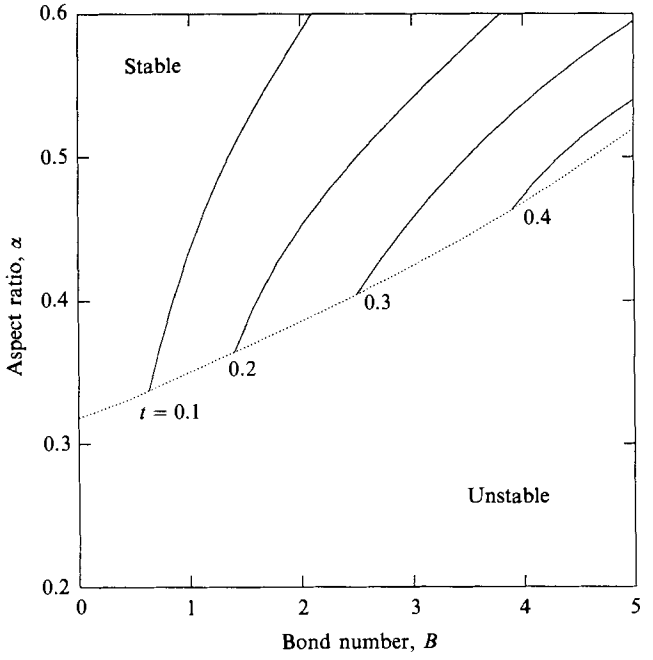

FIGURE 14. Stable and unstable operating regions for various values of the gravitational Bond number with the meniscus thickness as a parameter.

thicknesses. The dotted line represents the locus of the limit points in the upper branch of the first $\mu\delta$ bifurcating family. For values of the Bond number to the right of the solid lines the two interfaces touch each other.

5. Concluding remarks

A detailed picture of shape and stability of annular menisci subject to various external disturbances has been presented. These menisci are stable when their aspect ratio is between certain values that depend on their thickness, volume, external pressure and gravitational Bond number. Effects from each of the parameters separately have been examined using both asymptotic analysis and numerical simulation, with gratifying agreement. In particular, the asymptotic analysis presented in §3 is very useful in determining whether imperfections due to external parameters break or shift the bifurcation points. Extension of this methodology in order to examine simultaneous variations of several parameters is straightforward, and it may provide the limits of operation under these circumstances also.

The unperturbed annular menisci become unstable owing to a transcritical

bifurcation to reflectively symmetric shapes. Unstable modes resembling the ones that exist in the break-up of liquid jets arise for even smaller values of the aspect ratio and from subcritical families. Consequently, Rayleigh's (1979) analysis is not directly applicable for the present configuration. Furthermore, the dynamic behaviour of the menisci close to the first neutrally stable curve will closely resemble that of an electric drop close to the first critical point (Tsamopoulos *et al.* 1985). As was the case with the cylindrical jet, the instability is induced by surface tension forces. These forces become increasingly important as the radius of the inner surface becomes smaller.

All these results are valid when the axis of symmetry of the meniscus is vertical and the contact lines between the meniscus and the confining solid surfaces are fixed, circular and concentric. When, for example, owing to design requirements, the meniscus is tilted with respect to gravity or the two solid surfaces are misaligned, non-axisymmetric stable shapes will arise. All azimuthal asymmetries break the non-axisymmetric shape families. As noted in §4 a bifurcation point breaks only when imperfections develop that preserve the symmetry of the previously connected shape families.

One of the authors, J.A.T., was partially supported by the Fluid Mechanics Program of the National Science Foundation.

Appendix A

The inhomogeneous terms at second order in (3.4)–(3.6) for variations in γ are

$$d_{\mathrm{I}}^{(0,2)} = -\Big\{\frac{\mu}{2\delta}(2R_{\mathrm{I}}^{(0,1)}R_{\mathrm{I}zz}^{(0,1)} + (R_{\mathrm{I}z}^{(0,1)})^2) + 2\delta\alpha^{(0,1)}R_{\mathrm{I}zz}^{(0,1)} + \delta^2(B^{(0,2)}z + \Delta P^{(0,2)}) + \mu\delta(B^{(0,1)}z + \Delta P^{(0,1)} - P_{\mathrm{F}}^{(0,1)})R_{\mathrm{I}}^{(0,1)}\Big\},$$

$$d_{\mathrm{O}}^{(0,2)} = -\{\tfrac{1}{2}(2R_{\mathrm{O}}^{(0,1)}R_{\mathrm{O}zz}^{(0,1)} + (R_{\mathrm{O}z}^{(0,1)})^2) + 2\delta\alpha^{(0,1)}R_{\mathrm{O}zz}^{(0,1)} - \delta^2 B^{(0,2)}z + \delta^2(P_{\mathrm{F}}^{(0,1)} - B^{(0,1)}z)R_{\mathrm{O}}^{(0,1)}\},$$

$$d_{\mathrm{P}}^{(0,2)} = -\frac{1}{2}\Big\{\int_0^1 [(R_{\mathrm{O}}^{(0,1)})^2 - (R_{\mathrm{I}}^{(0,1)})^2]\,\mathrm{d}z - \Delta V^{(0,2)}\Big\}.$$

These inhomogeneous terms at third order are

$$\begin{aligned} d_{\mathrm{I}}^{(0,3)} = -\Big\{&\frac{\mu}{\delta}[R_{\mathrm{I}}^{(0,1)}R_{\mathrm{I}zz}^{(0,2)} + R_{\mathrm{I}z}^{(0,1)}R_{\mathrm{I}z}^{(0,2)} + \delta\alpha^{(0,1)}(R_{\mathrm{I}z}^{(0,1)})^2] \\ &+ 2\delta\alpha^{(0,1)}R_{\mathrm{I}zz}^{(0,2)} + \delta^2[B^{(0,3)}z + \Delta P^{(0,3)}] \\ &+ R_{\mathrm{I}zz}^{(0,1)}\Big[-\frac{3}{2\delta^2}(R_{\mathrm{I}z}^{(0,1)})^2 + \frac{\mu}{\delta}(R_{\mathrm{I}}^{(0,2)} + 2\delta\alpha^{(0,1)}R_{\mathrm{I}}^{(0,1)}) \\ &+ 2\delta(\alpha^{(0,2)} + \delta(\alpha^{(0,1)})^2)\Big] \\ &+ \mu\delta[(B^{(0,1)}z + \Delta P^{(0,1)} - P_{\mathrm{F}}^{(0,1)})R_{\mathrm{I}}^{(0,2)} \\ &+ (B^{(0,2)}z + \Delta P^{(0,2)} - P_{\mathrm{F}}^{(0,2)})R_{\mathrm{I}}^{(0,1)}]\Big\}, \\ d_{\mathrm{O}}^{(0,3)} = -\Big\{&R_{\mathrm{O}}^{(0,1)}R_{\mathrm{O}zz}^{(0,1)} + R_{\mathrm{O}z}^{(0,1)}R_{\mathrm{O}z}^{(0,2)} + \delta\alpha^{(0,1)}(R_{\mathrm{O}z}^{(0,1)})^2 \\ &+ 2\delta\alpha^{(0,1)}R_{\mathrm{O}zz}^{(0,2)} + \delta^2 B^{(0,3)}z \end{aligned}$$

$$+R_{\mathrm{O}zz}^{(0,1)}\left[-\frac{3}{2\delta^2}(R_{\mathrm{O}z}^{(0,1)})^2+R_{\mathrm{O}}^{(0,2)}+2\delta\alpha^{(0,1)}R_{\mathrm{O}}^{(0,1)}\right.$$

$$\left.+2\delta(\alpha^{(0,2)}+\delta(\alpha^{(0,1)})^2)\right]+\delta^2[(P_{\mathrm{F}}^{(0,1)}-B^{(0,1)}z)R_{\mathrm{O}}^{(0,2)}$$

$$\left.+(P_{\mathrm{F}}^{(0,2)}-B^{(0,2)}z)R_{\mathrm{O}}^{(0,1)}]\right\},$$

$$d_{\mathrm{P}}^{(0,3)}=-\int_0^1[R_{\mathrm{O}}^{(0,1)}R_{\mathrm{O}}^{(0,2)}-R_{\mathrm{I}}^{(0,1)}R_{\mathrm{I}}^{(0,2)}]\,\mathrm{d}z+\tfrac{1}{2}\Delta V^{(0,3)}.$$

For variations in ϵ the inhomogeneous terms are similar, except that $\Delta P=\Delta V=B=0$, and the superscript $(0,m)$ is substituted by $(n,0)$.

Appendix B

The coefficients I_0, I_1, I_2 in equation (3.25) are

$$I_0=\delta\xi^3(2\beta_1-\mu),\quad I_1=\delta^3(\xi^2\gamma_1+\gamma_2)-2(\xi^3\beta_1+\beta_2)$$

$$I_2=-4\delta^2(\xi^4\beta_1^3-\beta_2^3)+\delta\xi^3\beta_1^2(\xi+5\delta^2)-\delta\beta_2^2(1+5\delta^2)-6\xi^4\beta_1(\xi+3\delta^2)$$

$$+6\beta_2(1+3\delta^2)+3\delta(\xi^4-1)+9\delta^3(\xi^3-1)$$

For the μ bifurcating family the expression I_3, I_4 and I_5 in equation (3.31) are

$$I_3=\delta^2/\mu,\quad I_4=\delta\mu^2,\quad I_5=-\frac{\delta^2\alpha^{(2,0)}}{(\xi^2\alpha^{(0,0)})}.$$

For the δ family they are

$$I_3=-\delta,\quad I_4=\delta^3,\quad I_5=-\frac{\delta^2\alpha^{(2,0)}}{\alpha^{(0,0)}}.$$

REFERENCES

Abbott, J. P. 1978 An efficient algorithm for the determination of certain bifurcation points. *J. Comput. Appl. Math.* **4**, 19–26.

Boussinesq, J. 1869 *C. R. Acad. Sci. Paris* **69**, 128.

Brown, R. A. & Scriven, L. E. 1980 The shapes and stability of captive rotating drops. *Phil. Trans. R. Soc. Lond.* A **297**, 51–79.

Chandrasekhar, S. 1961 *Hydrodynamic and Hydromagnetic Stability*. Clarendon.

Esser, P. D., Paul, D. D. & Abdel-Khalik, S. I. 1981 Stability of the lithium "waterfall" first wall protection concept for inertial confinement fusion reactors. *Nucl. Technol./Fusion* **1**, 285–294.

Friedman, B. 1956 *Principles and Techniques of Applied Mathematics*. Wiley.

Hoffman, M. A., Takahashi, R. K. & Monson, R. D. 1980 Annular liquid jet experiments. *Trans. ASME* I: *J. Fluids Engng* **102**, 344–349.

Ioos, G. & Joseph, D. D. 1980 *Elementary Stability and Bifurcation Theory*. Springer.

Keller, H. B. 1977 Numerical solution of bifurcation and nonlinear eigenvalue problems. In *Applications of Bifurcation Theory* (ed. P. H. Rabinowitz), pp. 359–384. Academic.

Laplace, P. S. 1805 *Theory of Capillary Attraction*. Supplement to the tenth book of *Celestial Mechanics* (translated and annotated by N. Bowditch, 1839), 1966 reprint by Chelsea, New York.

Lee, C. P. & Wang, T. G. 1986 A theoretical model for the annular jet instability. *Phys. Fluids* **29**, 2076–2085.

MACSYMA 1977 *Reference Manual.* Laboratory of Computer Science, Massachusetts Institute of Technology.

MATKOWSKY, B. J. & REISS, E. L. 1977 Singular perturbations of bifurcations. *SIAM J. Appl. Maths* **33**, 230–255.

NAYFEH, A. H. 1970 Nonlinear stability of a liquid jet. *Phys. Fluids* **13**, 841–847.

PLATEAU, J. A. F. 1873 *Statique Expérimentale et Théorique des Liquides Soumix aux Seules Forces Moleculaires.* Gauthier-Villars.

RAYLEIGH, LORD 1879 On the stability of jets. *Proc. Lond. Math. Soc.* **10**, 4–13.

RAYLEIGH, LORD 1892 On the stability of cylindrical fluid surfaces. *Phil. Mag.* **34**, 177–180.

REISS, E. L. 1977 Imperfect bifurcation. In *Applications of Bifurcation theory* (ed. P. H. Rabinowitz), pp. 37–71. Academic.

STRANG, G. & FIX, G. J. 1973 *An Analysis of the Finite Element Method.* Prentice Hall.

THOMAS, P. D. & BROWN, R. A. 1987 LU decomposition of matrices with augmented dense constraints. *Int. J. Num. Meth. Engng* **24**, 1451–1459.

TSAMOPOULOS, J. A., AKYLAS, T. R. & BROWN, R. A. 1985 Dynamics of charged drop break-up. *Proc. R. Soc. Lond.* A **401**, 67–88.

UNGAR, L. H. & BROWN, R. A. 1982 The dependence of the shape and stability of captive rotating drops on multiple parameters. *Phil. Trans. R. Soc. Lond.* A **306**, 347–370.

YOUNG, T. 1805 Essay on the cohesion of fluids. *Phil. Trans. R. Soc. Lond.* A **95**, 65–87.